ON THE OPERATIONAL BEHAVIOR OF PACKED-BED THERMAL ENERGY STORAGE: A SECOND-LAW OF THERMODYNAMICS APPROACH TO DETERMINE THE INSTANTANEOUS ENERGY CONTENT

Ignacio Calderón-Vásquez[1]*, José M. Cardemil[1,2], Felipe G. Battisti[3]

[1]Department of Mechanical and Metallurgical Engineering, Escuela de Ingeniería, Pontificia Universidad Católica de Chile, Santiago, Chile
[2]Centro de Energía UC, Pontificia Universidad Católica de Chile, Santiago, Chile
[3]Departamento de Mecánica, Facultad de Ingeniería, Universidad Tecnológica Metropolitana, Santiago, Chile

*Corresponding Author: idcalderon@uc.cl

ABSTRACT

Packed-bed thermal energy storage (PBTES) systems have arisen as a promising alternative to store heat at high temperatures with low implementation costs. The literature has focused on improving its design to reduce thermal losses, enhance structural integrity, and increase storage capacity by analyzing thermocline development. The integration of PBTES systems has been a challenge due to the thermocline; such thermal gradient implies assessing the temperature limits of the applications to decide how to manage the PBTES charge and discharge processes. Nevertheless, this component's lack of monitoring indicators leads to undesired operation once integrated into the system. This article proposes a novel degradation parameter as a monitoring indicator for the PBTES operation. Through a second law of thermodynamics, different sources of exergy losses are collected into this parameter and compared to an ideal exergy stored/released rate. This article analyzes in depth the actual limits of the charging degradation and contrasts it to the utilization factor, a metric to evaluate the amount of useful energy discharged each cycle. This contrast is performed with a multi-objective optimization varying the cut-off temperature at charge/discharge and the charge/discharge temperature. The maximum limit for the charging degradation is around 0.35 to maximize the utilization factor when the system discharges from temperatures close to the environment. For that operational condition, the charging degradation limit can also be predicted with the cut-off charging temperature; therefore, its value can be set before its operation and used as a decision variable to manage the system's operation.

1 INTRODUCTION

Storing heat in a packed bed of rocks is a promising alternative to reduce the implementation costs of Thermal Energy Storage (TES) systems. This technology consists of solids arranged on a container with inlet ports, where a heat transfer fluid (HTF) can enter and leave the storage. As the fluid conveys heat with the solids, a thermocline develops inside the storage. The HTF transports the energy from the source to the TES or the TES to the demand. The main advantage of this technology is its simple implementation as it can employ natural rocks or industrial byproducts (Hänchen et al., 2011), the latter being a growth interest in the scientific community aiming to the valorization of wastes from metallurgical processes (Calderón-Vásquez et al., 2021; Rong et al., 2024; Ye et al., 2023). In that context, research has demonstrated that using industrial byproducts can reduce up to 35% of the TES component's implementation costs and enable storing heat at high temperatures when employing gaseous HTF (Agalit et al., 2020). These characteristics put the technology in interest for different energy applications: industrial waste heat recovery (Ortega-Fernández et al., 2019; Touzo et al., 2020), renewable electricity/heat (Promotionsausschuss & Von Der Heyde, 2022), and concentrating solar power (CSP) (Trevisan et al., 2021). Indeed, most studies are focused on the optimization of its performance and costs in terms of its design and sizing for CSP plants (Battisti et al., 2022; Marti et al., 2018; Trevisan et al., 2021), also the investigation of different container geometries to decrease thermal

https://doi.org/10.52202/077185-0002

and hydraulic losses (Calderón-Vásquez & Cardemil, 2024; McTigue & White, 2018; Trevisan et al., 2022). However, involving operational characteristics on PBTES systems to define a design that maximizes its utilization as a component and manages the thermocline development to avoid thermal losses is a relevant issue that has not been addressed yet (He et al., 2022). It is fundamental to develop a complete integration of PBTES as a component on energy systems.

(Ortega-Fernández et al., 2019) developed a discussion regarding the operation strategies and management of the thermal behavior of PBTES systems. The article compared three operating modes for a specific industrial application in terms of the thermal and material efficiency of the storage. These operating modes correspond to: (1) Complete charge-discharge, (2) Limited-time operation, and (3) Limited-temperature operation. The latter is a strategy commonly employed to constrain the component when integrated into CSP plants (Battisti et al., 2022; Trevisan et al., 2021) and retain the thermocline inside the storage to maximize the TES's utilization (Geissbühler et al., 2019). The operational limitation of the PBTES temperature is applied with a restriction on the measured outlet temperature, a variable easily monitored and controlled. This restriction is called "cut-off" temperature and could differ for the charge and discharge process.

Despite the temperature constraints, deciding whether to charge or discharge the packed bed has to be based on an indicator that reveals the actual energy content of the system. For instance, after a period of charge interrupted by source fluctuations, discharging could not be possible if the energy stored is not enough for the application; therefore, the system will remain idle, degrading its energy content by diffusion, thermal losses, and mixing (Haller et al., 2009). Trevisan et al. (2020) assessed the implementation of different operating modes of an integrated PBTES for a sCO_2 Brayton Power Cycle with the state-of-charge (SOC) of the PBTES as the tool for decision-making in the system's control logic. The SOC is a ratio between the instantaneous energy content of the TES and the maximum energy capacity, mostly determined by the maximum operating temperature difference. The disadvantage of employing such an indicator is that increasing its value implies operating the system close to fully charged, decreasing the PBTES's thermal efficiency as the outflow energy rises on time (Ortega-Fernández et al., 2019).

Defining an indicator that provides information about the actual system's capacity is crucial from an operational perspective. It should be aligned with the packed-bed system's desirable operation, corresponding to minimizing the amount of outflow energy to maximize its cyclic utilization and efficiency. To date, there is no operational indicator in the state-of-the-art with that characteristics as described on the SOC disadvantages. Hence, the present study proposes a novel approach to characterize the dynamic behavior of the operational characteristics of a PBTES. By applying the second law of thermodynamics, a strategy to determine the degradation of the useful work in the system is employed to compute an operational indicator to monitor such variable in time. This parameter is contrasted with the PBTES outflow temperature and the SOC, the other indicator used to assess operating strategies for control logic on integrated PBTES systems. The work also analyzes the impact on varying operational variables, such as charging/discharging temperature and cut-off temperatures of both processes, independent of the PBTES sizing. Finally, through a multi-objective optimization, the article aims to define the actual degradation limits of an operating PBTES to maximize its utilization; therefore, it contributes to defining an operational constraint of the system to minimize the degradation of the useful work contained.

2 METHODOLOGY

The research considers a packed-bed thermal energy storage system consisting of rocks contained in a cylindrical thermocline storage tank. The storage operates between two boundaries: a heat source at temperature T_H and a heat sink at temperature T_L ($T_H > T_L$). Additionally, the storage can exchange heat with the environment at temperature T_∞.

During the TES's charging process, the heat transfer fluid flows from the heat source at T_H to the tank's top part, flowing through the porous medium, transferring heat and exiting the system at a lower temperature. Conversely, in the discharging process, the fluid enters the storage from the heat sink at T_L and recovers the heat stored in the solids, increasing its temperature, discharging the energy to the

https://doi.org/10.52202/077185-0002

source which can be used for any process. The heating/cooling stages of the fluid and solid phases are modeled through an energy balance of each phase, considering diffusion, convection between the fluid and solids, and thermal losses through the storage wall. The details regarding the assumptions and mathematical formulation of the model had been previously published by our research group (Battisti et al., 2021; Calderón-Vásquez & Cardemil, 2024). Both articles include an in-depth analysis of thermal loss modeling and validation with CFD modeling for sCO_2 applications (Battisti et al., 2021) and experimental data for air-solid systems (Calderón-Vásquez & Cardemil, 2024). According to Battisti et al. (2021), the numerical results are consistent with the CFD experiments developed by Johnson et al. (2018), which correspond to a PBTES system of 70 MWh of design capacity. Conversely, the model's validation performed by Calderón-Vásquez & Cardemil (2024) presented a maximum error of 10 °C compared to the experimental data described, corresponding to an air-solid PBTES with 6 kWh of design capacity (Hänchen et al., 2011). Therefore, both models are validated on different storage scales and HTF.

The model provides information on the fluid and solid temperature profile inside the TES at any given operating time, particularly the transient evolution of the outlet's energy. The latter is a relevant variable from a component perspective since the outlet interacts with the heat source and sink. Monitoring the outlet temperature is crucial to estimate the useful work released from the TES to the sink or discharged from the TES to a process. Likewise, having information about the available exergy in the TES is important to decide whether to charge/discharge. A thermodynamic analysis is presented in the following subsection to provide a complete understanding of the temporal variations of the stored and released exergy and how it is degraded in each TES's operating cycle.

2.1 Thermodynamic analysis

Consider the same packed-bed domain from above. An exergy balance can be performed on the control volume as follows:

$$\left(\frac{dX}{dt}\right)_{CV} = \dot{X}_{in} - \dot{X}_{out} - \int_{CV} \left(1 - \frac{T_\infty}{T}\right) \dot{q}''' dV - \dot{X}_d \tag{1}$$

The first two terms of the R.H.S correspond to the exergy rate injected/extracted to/from the packed bed during the charge/discharge processes, the third term is the exergy loss through storage walls due to the temperature difference with the surroundings $\dot{X}_{HL}$, and the last term is the exergy destroyed. Defining $\dot{X}_H$ and $\dot{X}_L$ as the exergy rates calculated at the temperatures T_H and T_L, respectively, and $\dot{X}_{max} = \dot{X}_H - \dot{X}_L$ as the maximum exergy rate available to be supplied/extracted to/from the TES, Equation (1) can be rewritten for the charging process as

$$\left(\frac{dX}{dt}\right)_{CV} = \dot{X}_{max} - \dot{X}_{outflow,ch} - \dot{X}_{HL} - \dot{X}_d \tag{2}$$

where $\dot{X}_{outflow,ch} = \dot{X}_{out} - \dot{X}_L$ is the exergy released from the control volume during the charging process due to "early" discharge of the thermocline. Through Equation (2), it can be concluded that the maximum exergy is degraded by different sources, idealizing that maximum as a stream that enters the TES at T_H and exits at T_L. The charging degradation parameter DP_{ch} is therefore defined as:

$$DP_{ch} = \frac{\dot{X}_{outflow,ch} + \dot{X}_{HL} + \dot{X}_d}{\dot{X}_{max}} \tag{3}$$

This novel definition corresponds to a ratio between the exergy "leaks" that occur during the charging process and the ideal scenario of exergy charging to the storage; thus, DP_{ch} indicates how far the storage is from the boundaries regarding useful energy.

The formulation is slightly different for the discharging process, since the target is to recover exergy, in contrast to the charging process, whose is to store; hence, the degradation should be oriented to the capability to keep the exergy or spread it through other mechanisms. Considering Equation (1), the inlet exergy is at T_L, while the outlet temperature decreases with time as the packed bed cools. The exergetic "penalization" can be calculated with $\dot{X}_{outflow,dch} = \dot{X}_H - \dot{X}_{out}$. Equation (3) can be rewritten by rearranging its terms as:

$$\left(\frac{dX}{dt}\right)_{CV} + \dot{X}_{HL} + \dot{X}_d = \dot{X}_{outflow,dch} - \dot{X}_{max} \tag{4}$$

https://doi.org/10.52202/077185-0002

Equation (4) can be interpreted as establishing that the maximum exergy released by the ideal discharging process is affected by the outflow temperature below the target temperature. The other exergy loss terms are considered as different ways to discharge the system, but they are not directly perceived by the demand/application of the TES's released exergy. Consequently, the discharging degradation parameter corresponds to the following:

$$DP_{dch} = \frac{\dot{X}_{outflow,dch}}{\dot{X}_{max}} \tag{5}$$

2.2 Application of the System's degradation parameters

The definition of these novel instantaneous parameters, available in Equation (3) and (5), enables monitoring the actual storage capacity's degradation when the system is charging or discharging. Nevertheless, the limits of the degradation parameters must be explored to ensure an operation aligned with maximizing the system's utilization. According to Geissbühler et al. (2019), the degradation of the PBTES is associated with the thermocline flattening, and it can be assessed through a performance indicator called the utilization factor (ζ), which is defined as

$$\zeta = \frac{\int_V (\rho c_p)_s \left(T(V, t_{end,ch}) - T(V, t_{end,dch})\right) dV}{(1-\varepsilon)(\rho c_p)_s V_{TES}(T_H - T_L)} \tag{6}$$

The numerator is the utilized storage capacity, determined by integrating the energy stored at the end of the charging process minus the remaining energy at the end of the discharging process, and the denominator is the maximum storage capacity. In Equation (6), $(\rho c_p)_s$ is the solid's capacitance, V_{TES} the TES internal volume, and ε the porous medium void fraction.

Assuming that there are degradation limits, the control logic should consider the operation of any PBTES process until the limit is reached, like the implementation of the SOC included by Trevisan et al. (2020) that aligns with source and demand requirements. However, the SOC provides information about the energy content integrating the temperature gradient inside the PBTES each time, which could lead to misinterpretation regarding the temperature levels within the storage. For instance, the charging process could be extended for periods during which the thermocline has been partially expelled from the tank, affecting the utilization factor and overconsuming power to keep the air flowing through the PBTES (Calderón-Vásquez & Cardemil, 2024; Geissbühler et al., 2019).

2.3 Case study

A simple case study is proposed to investigate the actual limits of the PBTES degradation. Aiming to assess how the operating conditions impact the system's dynamics, the variables of this study will be the cut-off temperature and the inlet temperature for the charge and discharge ($\Delta T_{co,ch}$, $\Delta T_{co,dch}$, T_H, and T_L, respectively). The cut-off temperature ranges proposed on Table 1 follows the typical configurations for CSP plants (Trevisan et al., 2021). The thermal power demand and the design discharging time are fixed at 1 MW and 12 hours; hence, for any pair T_H and T_L, a PBTES system is sized according to the methodology presented by Trevisan et al. (2021). The simulation of the PBTES charge-discharge process will be controlled by $\Delta T_{co,ch}$ and $\Delta T_{co,dch}$ and the degradation parameters will be computed using the simulation's transient results. Figure 1 shows the workflow of the case study simulation. After the design, a cyclic simulation of the PBTES system is developed, considering a system's initialization to monitor the charging process condition, similar to a PBTES operation and using a partial load of the mass flow rate, since the TES is usually employed to store the energy surplus for renewable generation. The cut-off criteria for the charge and discharge are only limiting temperatures at the PBTES outlet.

Defining the limits of the degradation parameters is a task that will lead to including them as metrics to manage the PBTES operation. The charging process conceptualization involves operating the system while keeping the DP_{ch} small, since the instantaneous exergetic losses remain low. However, this could conflict with maximizing the utilization factor, which increases when deep charge and discharge periods occur. On the other hand, DP_{dch} is an indicator that depends on the outflow temperature, variable that is monitored during the PBTES operation; hence, its minimization depends directly on the discharge

https://doi.org/10.52202/077185-0002

depth. Also, if the operating temperature limits during discharge are known, the DP_{dch} limits are known as well. A multi-objective optimization determines the influence of operational parameters on DP_{ch} at the end of the charging period and the utilization factor ζ. As a result, the solution set is a combination of operational parameters that minimizes the PBTES degradation and maximizes its utilization. Table 1 shows the multi-objective optimization formulation, the algorithm employed, and the tuning parameters. The optimization considers the variables in the population as inputs for the design and simulation processes, as indicated in Figure 1.

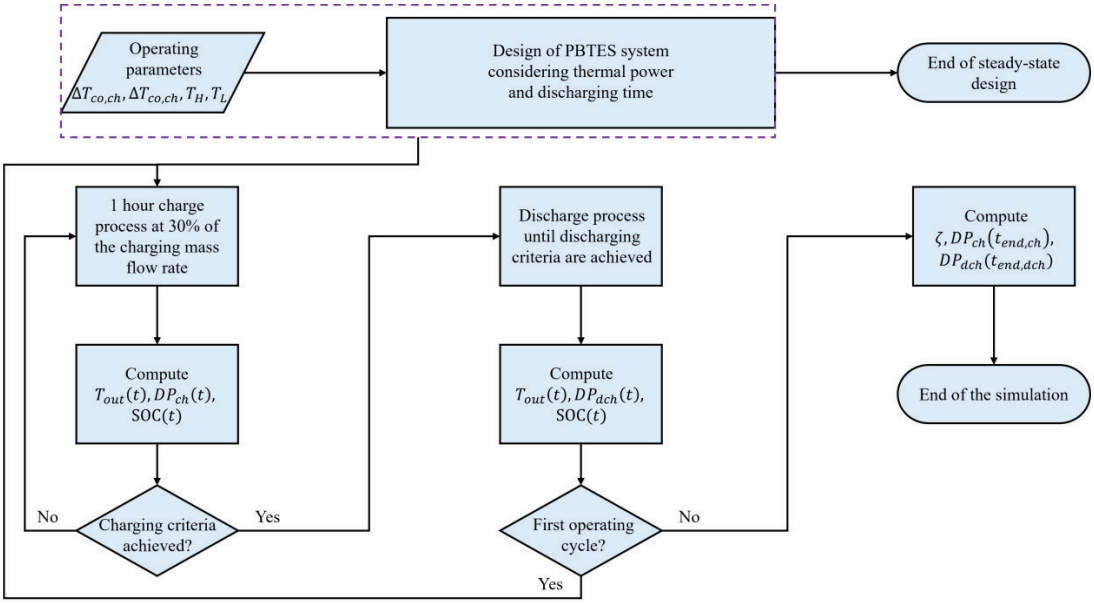

Figure 1: Scheme of the case study workflow.

Table 1: Parameters of the multi-objective optimization.

Parameter		Value
Multi-objective functions		$\min DP_{ch}(t_{end,ch})$ $\max \zeta$
Design variables	Cut-off temperature at the charge	$\Delta T_{co,ch} \in [20, 200]$ °C
	Cut-off temperature at the discharge	$\Delta T_{co,dch} \in [20, 100]$ °C
	Charging temperature	$T_H \in [400, 700]$ °C
	Discharging temperature	$T_L \in [25, 300]$ °C
Restrictions		$T_L + \Delta T_{co,ch} < T_H$ $T_L < T_H - \Delta T_{co,dch}$
Algorithm		Non-Dominated Sorting Genetic Algorithm (NSGA-II)
Population size		50
Number of generations		50

3 RESULTS AND DISCUSSION

Figure 2 shows the monitoring indicators of the PBTES operation along the time for both charging and discharging processes: the dimensionless outlet temperature $\theta_{out} = \frac{T_{out}(t) - T_\infty}{T_H - T_\infty}$, the SOC, and the DP.

https://doi.org/10.52202/077185-0002

The extension of the charging period is due to the low mass flow rate, whereas the short discharging process is caused by the increase of the mass flow rate, considering the thermal power requirements for the PBTES design. As explained above, during the charging process the PBTES's outflow temperature increases over time because of the thermal front propagation along the domain. As observed in Figure 2, the degradation parameter and SOC increase as well, but their responses differ between each indicator. The SOC behaves like a linear function since it is the energy stored at any time. For this case, the SOC does not start at zero because some energy remains from the previous cycles. In contrast, DP_{ch} increases accordingly to the outflow temperature. The behavior corresponds to an exponential increase, being slow during most of the charging process and rapidly increasing near the cut-off condition. This is due to the thermocline release out from the PBTES, a state far from the desired stratified condition represented by $\dot{X}_{max}$. For the discharging period, the outflow temperature is monitored between the PBTES and demand. This temperature will decrease from the maximum temperature level in the PBTES to the cut-off condition. The SOC also decreases as now the stored energy is released. The DP_{dch}, on the other hand, increases over time because of the reduction of the outflow temperature, enlarging the gap between the objective temperature T_H and T_{out}.

The interpretation of these monitoring indicators depends on the process taking place. For the charge, the SOC increment indicates a growth in the system's stored energy. For the discharge, the SOC decrease results from the energy extraction from the system, but there is not a clear picture regarding the actual potential of this energy in terms of its temperature during both processes. Now, the degradation parameter increases in both cases. The degradation for the charging process regards its potential to store heat, mainly represented by the outflow temperature. When the domain has been heated completely at temperatures higher than T_L, its maximum storage potential (i.e., $\dot{X}_{max}$) is lower, representing a degradation starting point since less exergy is stored in the control volume. For the discharging process, the degradation regards the system's capability to release exergy at the application temperature constraint, and it follows the inverse shape of the PBTES's outflow temperature.

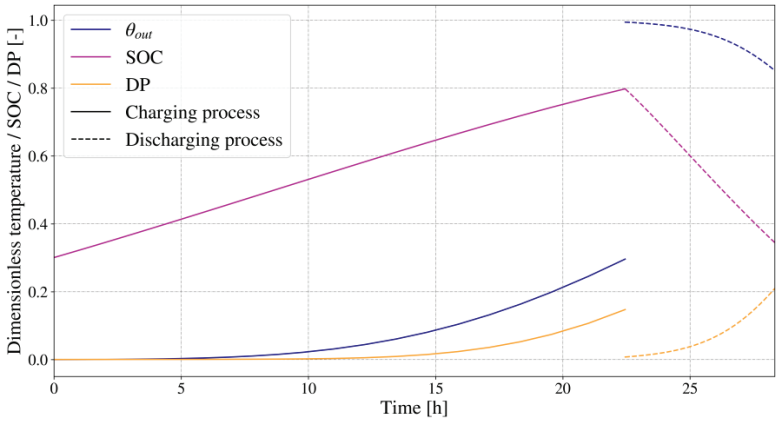

Figure 2: PBTES operation in time. Results for $\Delta T_{co,ch} = 200$°C, $\Delta T_{co,dch} = 100$°C, $T_H = 700$°C, and $T_L = 25$°C.

Figures 3 and 4 present the results regarding the multi-objective optimization. The Pareto front results from the conflict between the utilization factor and the degradation parameter evaluated at the end of the charging process, i.e., $DP_{ch}(t_{end,ch})$. The color of each point located on the Pareto front indicates the value of $\Delta T_{co,ch}$. As observed in Figure 3, as the utilization factor increases, the system final degradation increases as well, as a response to the cut-off limit required to enlarge the charging depth. Overall, the degradation limit to obtain a maximum utilization factor is around 0.35. Also, the points located at the lower left zone minimize the degradation parameter with a utilization factor of 0.3. Despite having a low utilization factor, values on the Pareto front demonstrate that it is possible to operate the PBTES at low degradation ranges. However, based on those points, there is a configuration that enlarges the utilization factor that is mainly related to a greater cut-off temperature limit during charging process. Figure 4 shows the distribution of the design variables along the Pareto front. The

https://doi.org/10.52202/077185-0002

cut-off temperature of the charging process is the main variable that provokes the conflict between the two objective functions. On the other hand, the distributions of $\Delta T_{co,dch}$, T_H, and T_L are clustered at the upper, lower, and lower bounds of each variable, respectively. Such behaviors are due to the following reasons:

- Operating at high charge and discharge temperatures increases the thermal losses, as the thermocline develops at temperatures higher than T_∞. The power loss through that mechanism affects the degradation of the PBTES system, increasing DP_{ch}.
- The cut-off discharging temperature is a variable that influences the utilization factor. Operating the PBTES system at high values of $\Delta T_{co,dch}$ increases the discharging depth and the movement of the thermocline between consecutive cycles.
- Developing the discharging process at temperatures close to the environment ($T_L = 25$℃) enables the thermocline to operate in a temperature range closer to the reference T_∞ in the lower bound. Therefore, the degradation during the charging process always starts near to zero and without residual outflow potential from previous cycles.

Overall, the distribution of the design variables states that $\Delta T_{co,dch}$, T_H, and T_L are not relevant to the conflict between the proposed objective functions, being $\Delta T_{co,ch}$ the only variable spread across the whole domain. Such result is expected since the degradation parameter is calculated from the charging operating conditions.

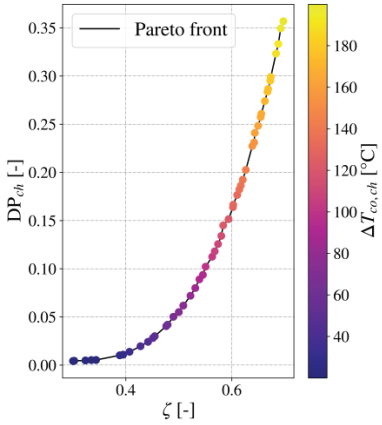

Figure 3: Pareto front resulting from the multi-objective optimization.

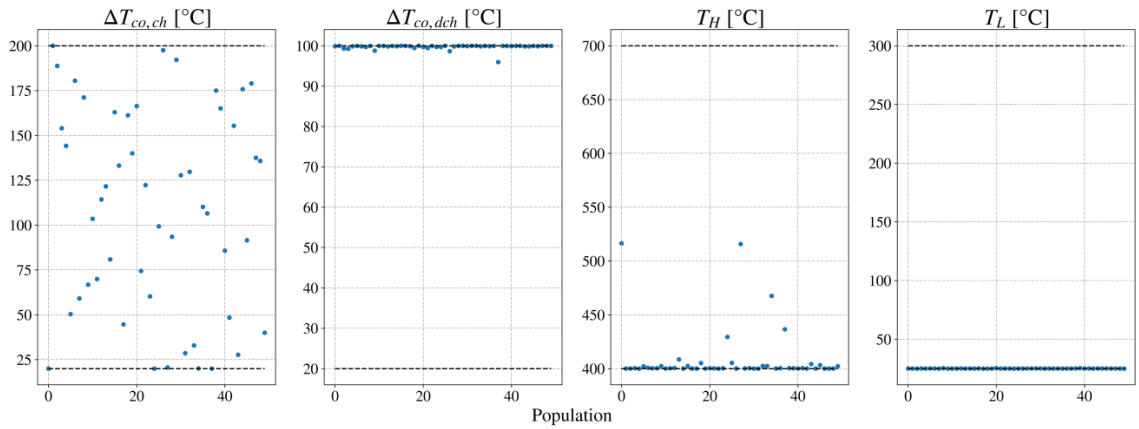

Figure 4: Pareto front population's design variables.

Through a sensitivity analysis one may explore how the charging temperature, affects the Pareto front development. As observed in Figure 5-a, increasing the operational charging temperature decreases the maximum limit of the degradation parameter. This is a consequence of fixing the thermal power

https://doi.org/10.52202/077185-0002

demand; thus, the required TES volume for a larger $\Delta T = T_H - T_L$ decreases when T_H increases. As a result, the degradation due to thermal losses and exergy destruction decreases, contributing less to DP_{ch}. This is confirmed by the center plot of Figure 5-b, where the cut-off temperature is plotted against $DP_{ch}(t_{end,ch})$. For the same value of $\Delta T_{co,ch}$, $DP_{ch}(t_{end,ch})$ increases when the charging temperature decreases. The latter is caused by the small temperature difference within the packed bed when the charging process occurs, flattening the temperature profile that ranges from $T_L + \Delta T_{co,ch}$ to T_H.

To perform a unification with the charging temperature and its cut-off limit, the dimensionless variable $\Delta\theta_{co,ch} = \frac{T_L + \Delta T_{co,ch} - T_\infty}{T_H - T_\infty}$ is computed. The idea is to collect the variations of $\Delta T_{co,ch}$ and T_H into a parameter that express the relative differences of one temperature interval against the other. As a result, the $DP_{ch}(t_{end,ch})$ becomes dependent only on $\Delta\theta_{co,ch}$ and all the cases for T_H remain on a similar distribution modeled through a power-law correlation, i.e., $DP_{ch}(t_{end,ch}) = a\,(\Delta\theta_{co,ch})^b$ (see Figure 5-c). The parameters resulting from the curve-fitting and the R^2 are presented in Table 2. This relationship makes it possible to estimate the systems' degradation limit by having information about the charging temperature and the cut-off charge limit. This correlation is specifically for $T_L = 25$℃ and $\Delta T_{co,dch} = 100$℃.

The same sensitivity analysis was performed for $T_L = 300$℃ with remarkable differences regarding the distribution of the points and the relationship between the variables. First, in Figure 6-a, it is observed that the curve order that relates ζ with $DP_{ch}(t_{end,ch})$ is reversed: decreasing the charging temperature enlarges the maximum limit of the charging degradation parameter, even resulting in values close to 1.0. This is a result of a fully-charged operating condition, and no thermocline is developed at all within the tank at the end of the charging process. This is also relevant as that scenario provides the worst utilization factors for the design variables combination. For higher charging temperatures, the degradation limit decreases since there is a thermocline developed within the storage and also increases the utilization factor. Still, the relationship between $\Delta T_{co,ch}$ and $DP_{ch}(t_{end,ch})$ remains as increasing functions, a phenomenon explained below (see Figure 6-b). However, the function $DP_{ch}(t_{end,ch})$ cannot be correlated only to $\Delta\theta_{co,ch}$ (Figure 6-c).

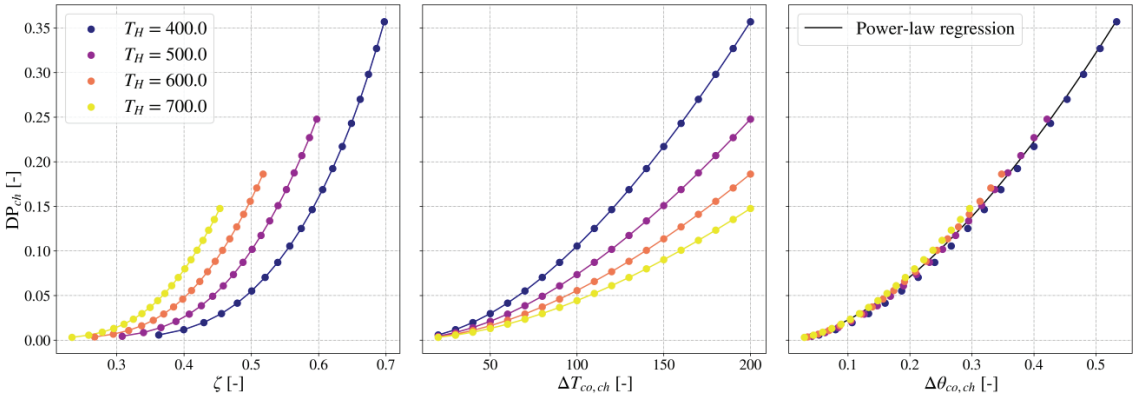

Figure 5: Sensitivity analysis for the charging temperature at $T_L = 25$℃ and $\Delta T_{co,dch} = 100$℃. (a) Objective functions, (b) relationship between the charging cut-off temperature and DP_{ch} at $t_{end,ch}$, and (c) relationship between the dimensionless cut-off charging temperature and DP_{ch}. at $t_{end,ch}$.

Table 2: Coefficients from the power-law regression.

Equation	a	b	R^2
$DP_{ch}(t_{end,ch}) = a\,(\Delta\theta_{co,ch})^b$	1.011	1.651	0.997

https://doi.org/10.52202/077185-0002

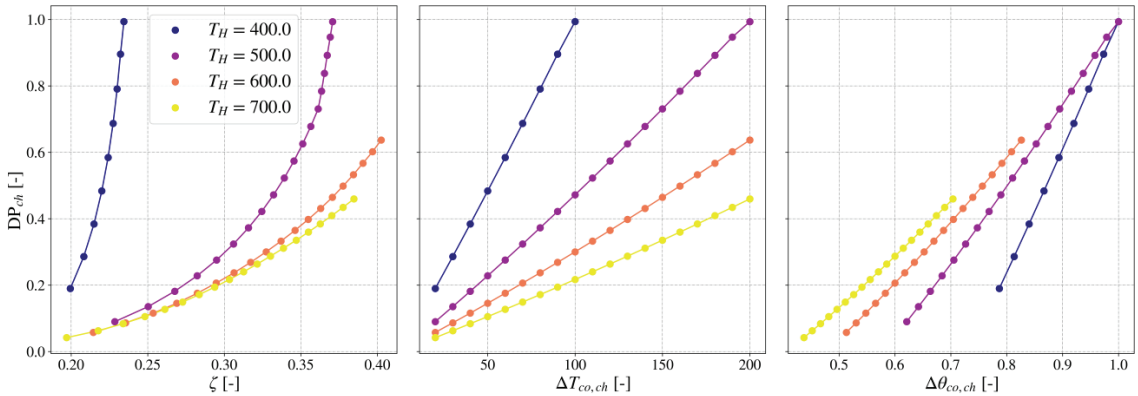

Figure 6: Sensitivity analysis for the charging temperature at $T_L = 300$℃ and $\Delta T_{co,dch} = 100$℃. (a) Objective functions, (b) relationship between the charging cut-off temperature and DP_{ch} at $t_{end,ch}$, and (c) relationship between the dimensionless cut-off charging temperature and DP_{ch}.

The statements regarding the relationship between the cut-off charging temperature and the degradation parameter limit $DP_{ch}(t_{end,ch})$ can be explained with Figures 7-a and 7-b. The colored rectangle represents the temperature range in which the charging temperature stops in the sensitivity analysis, varying $20℃ \leq \Delta T_{co,ch} \leq 200℃$. In Figure 7-a, the parabolic-like behavior indicates that the system´s thermal inertia retains the heat within the storage after releasing the thermocline after surpassing a limit $\Delta\theta_{co,ch} \approx 0.1$ or $\Delta T_{co,ch} \approx 70℃$ Then, the increase of the outflow temperature is approximately linear, and DP_{ch} grows at the same rate over time. This behavior is not the same when the discharging temperature is above the dead-state temperature (i.e., over T_∞), which is shown in Figure 7-b. The rapid growth of the degradation parameters is caused by the temperature difference between T_∞ and T_L. The outflow temperature is always higher than the dead-state condition; thus, the exergy rates are larger. As a result, DP_{ch} does not follow the same growing rate as the outlet temperature, and its limit cannot be modeled only with $\Delta\theta_{co,ch}$.

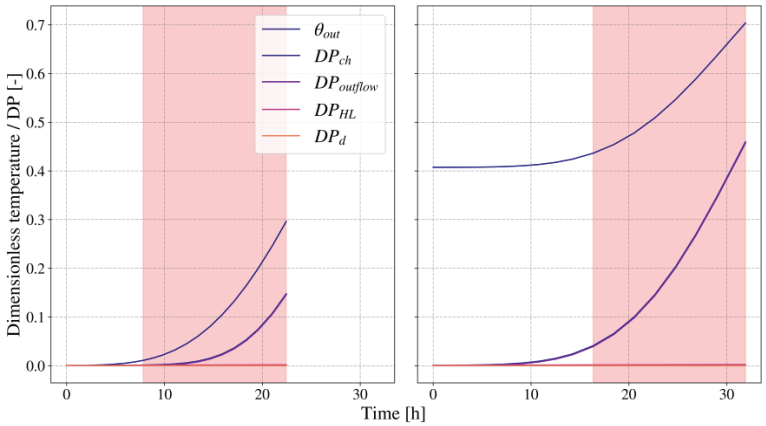

Figure 7: Dimensionless temperature and degradation in time during the charging process considering $\Delta T_{co,ch} = 200℃$, $\Delta T_{co,dch} = 100℃$, and $T_H = 700℃$. Plots for (a) $T_L = 25℃$ and (b) $T_L = 300℃$.

4 CONCLUSIONS

The present work assesses the operational behavior and dynamics of a PBTES system in terms of the second law of thermodynamics. Through the definition of a maximum state of exergy rate to be stored and released, the study proposes a degradation parameter DP to monitor the system's operation. This was contrasted with the SOC, another figure of merit proposed in the

https://doi.org/10.52202/077185-0002

literature to monitor the PBTES behavior. Through a sensitivity analysis and a multi-objective optimization, the limit value of this degradation parameter was explored. The major findings are listed below:

- The degradation parameter for both charging and discharging processes follow the PBTES instantaneous outlet temperature. The greater the DP, the less the instantaneous capacity to store/release exergy at the conditions set for charge/discharge. In contrast to the SOC, which indicates a maximum capacity when the PBTES has released the thermocline, the degradation depends on the thermocline movement.
- Multi-objective optimization of $DP_{ch}\left(t_{end,ch}\right)$ and the utilization factor revealed that the PBTES system should operate by setting the discharging temperature close to the environment In contrast, the actual conflict between the objective functions is caused by the cut-off charging temperature. High values of such a variable enhance the utilization factor, but also increase the final system's degradation when charging.
- The sensitivity study on the charging temperature revealed that the maximum degradation limit that maximizes the utilization factor is around 0.35 when $\Delta T_{co,ch} = 200$℃, $\Delta T_{co,dch} = 100$℃, $T_H = 400$℃, and $T_L = 25$℃. However, the degradation limit in the charge $DP_{ch}\left(t_{end,ch}\right)$ can be correlated with the dimensionless cut-off temperature when the discharging temperature is equal to the environment, predicting its value given a cut-off temperature condition to include it into a control logic for the system's management.

Further work should explore the effects on both operational and design conditions under these degradation parameters and analyze in depth how to relate the cut-off conditions with the charging limits when the discharging process is at temperatures higher than the environment. In addition, the discharging degradation parameter should be assessed using the proposed methodology. Overall, this study performs an introductory analysis to remark on the potential of these parameters to monitor the system's operation.

REFERENCES

Agalit, H., Zari, N., & Maaroufi, M. (2020). Suitability of industrial wastes for application as high temperature thermal energy storage (TES) materials in solar tower power plants – A comprehensive review. *Solar Energy*, *208*, 1151–1165. https://doi.org/10.1016/j.solener.2020.08.055

Battisti, F. G., de Araujo Passos, L. A., & da Silva, A. K. (2021). Performance mapping of packed-bed thermal energy storage systems for concentrating solar-powered plants using supercritical carbon dioxide. *Applied Thermal Engineering*, *183*, 116032. https://doi.org/10.1016/j.applthermaleng.2020.116032

Battisti, F. G., de Araujo Passos, L. A., & da Silva, A. K. (2022). Economic and environmental assessment of a CO2 solar-powered plant with packed-bed thermal energy storage. *Applied Energy*, *314*, 118913. https://doi.org/10.1016/j.apenergy.2022.118913

Calderón-Vásquez, I., & Cardemil, J. M. (2024). A comparison of packed-bed flow topologies for high-temperature thermal energy storage under constrained conditions. *Applied Thermal Engineering*, *238*, 121934. https://doi.org/10.1016/j.applthermaleng.2023.121934

Calderón-Vásquez, I., Segovia, V., Cardemil, J. M., & Barraza, R. (2021). Assessing the use of copper slags as thermal energy storage material for packed-bed systems. *Energy*, *227*. https://doi.org/10.1016/j.energy.2021.120370

Geissbühler, L., Mathur, A., Mularczyk, A., & Haselbacher, A. (2019). An assessment of thermocline-control methods for packed-bed thermal-energy storage in CSP plants, Part 1: Method descriptions. *Solar Energy*, *178*, 341–350. https://doi.org/10.1016/j.solener.2018.12.015

Haller, M. Y., Cruickshank, C. A., Streicher, W., Harrison, S. J., Andersen, E., & Furbo, S. (2009). Methods to determine stratification efficiency of thermal energy storage processes – Review and

https://doi.org/10.52202/077185-0002

theoretical comparison. *Solar Energy*, *83*(10), 1847–1860. https://doi.org/10.1016/j.solener.2009.06.019

Hänchen, M., Brückner, S., & Steinfeld, A. (2011). High-temperature thermal storage using a packed bed of rocks – Heat transfer analysis and experimental validation. *Applied Thermal Engineering*, *31*(10), 1798–1806. https://doi.org/10.1016/j.applthermaleng.2010.10.034

He, X., Qiu, J., Wang, W., Hou, Y., Ayyub, M., & Shuai, Y. (2022). A review on numerical simulation, optimization design and applications of packed-bed latent thermal energy storage system with spherical capsules. *Journal of Energy Storage*, *51*, 104555. https://doi.org/10.1016/j.est.2022.104555

Johnson, E., Bates, L., Dower, A., Bueno, P. C., & Anderson, R. (2018). Thermal energy storage with supercritical carbon dioxide in a packed bed: Modeling charge-discharge cycles. *The Journal of Supercritical Fluids*, *137*, 57–65. https://doi.org/10.1016/J.SUPFLU.2018.03.009

Marti, J., Geissbühler, L., Becattini, V., Haselbacher, A., & Steinfeld, A. (2018). Constrained multi-objective optimization of thermocline packed-bed thermal-energy storage. *Applied Energy*, *216*, 694–708. https://doi.org/10.1016/J.APENERGY.2017.12.072

McTigue, J. D., & White, A. J. (2018). A comparison of radial-flow and axial-flow packed beds for thermal energy storage. *Applied Energy*, *227*, 533–541. https://doi.org/10.1016/j.apenergy.2017.08.179

Ortega-Fernández, I., Uriz, I., Ortuondo, A., Hernández, A. B., Faik, A., Loroño, I., & Rodríguez-Aseguinolaza, J. (2019). Operation strategies guideline for packed bed thermal energy storage systems. *International Journal of Energy Research*, *43*(12), 6211–6221. https://doi.org/10.1002/ER.4291

Promotionsausschuss, V., & Von Der Heyde, M. (2022). *Electric thermal energy storage based on packed beds for renewable energy integration*. https://doi.org/10.15480/882.4165

Rong, Y., Huang, S. Y., & Zhou, H. (2024). Experimental study on storage performance of packed bed solar thermal energy storage system using steel slag. *Journal of Energy Storage*, *78*, 110042. https://doi.org/10.1016/j.est.2023.110042

Touzo, A., Olives, R., Dejean, G., Pham Minh, D., El Hafi, M., Hoffmann, J. F., & Py, X. (2020). Experimental and numerical analysis of a packed-bed thermal energy storage system designed to recover high temperature waste heat: an industrial scale up. *Journal of Energy Storage*, *32*, 101894. https://doi.org/10.1016/J.EST.2020.101894

Trevisan, S., Guédez, R., & Laumert, B. (2020). Thermo-economic optimization of an air driven supercritical CO2 Brayton power cycle for concentrating solar power plant with packed bed thermal energy storage. *Solar Energy*, *211*, 1373–1391. https://doi.org/10.1016/J.SOLENER.2020.10.069

Trevisan, S., Jemmal, Y., Guedez, R., & Laumert, B. (2021). Packed bed thermal energy storage: A novel design methodology including quasi-dynamic boundary conditions and techno-economic optimization. *Journal of Energy Storage*, *36*, 102441. https://doi.org/10.1016/J.EST.2021.102441

Trevisan, S., Wang, W., Guedez, R., & Laumert, B. (2022). Experimental evaluation of a high-temperature radial-flow packed bed thermal energy storage under dynamic mass flow rate. *Journal of Energy Storage*, *54*, 105236. https://doi.org/10.1016/j.est.2022.105236

Ye, C., Zhang, M., Yang, S., Mweemba, S., Huang, A., Liu, X., & Zhang, X. (2023). Application of copper slags in encapsulating high-temperature phase change thermal storage particles. *Solar Energy Materials and Solar Cells*, *254*, 112257. https://doi.org/10.1016/j.solmat.2023.112257

ACKNOWLEDGEMENT

The authors would like to thank the financial support from projects ANID/FONDEF/ID22I10200, ANID/FONDECYT/1231186, and ANID/FONDAP 1523A0006 ‘‘Solar Energy Research Center’’ - SERC - Chile. In addition, I. Calderón-Vásquez would like to acknowledge the PhD. Scholarship ANID-PFCHA/Doctorado Nacional/2021–21210778, and F. G. Battisti acknowledges the support from ANID/CONICYT through FONDECYT Postdoctorado 2022–#3220792.

https://doi.org/10.52202/077185-0002